Spectrochimica Acta Part A: Molecular and Biomolecular Spectroscopy 229 (2020) 117972

Contents lists available at ScienceDirect

Spectrochimica Acta Part A: Molecular and Biomolecular Spectroscopy

journal homepage: www.elsevier.com/locate/saa

Fluorescence biosensor based on silicon quantum dots and 5,5′-dithiobis-(2-nitrobenzoic acid) for thiols in living cells

Bo-Hui Huang [1], San-San Shen, Na Wei, Xiao-Feng Guo [1], Hong Wang *

Key Laboratory of Analytical Chemistry for Biology and Medicine (Ministry of Education), College of Chemistry and Molecular Sciences, Wuhan University, Wuhan 430072, China

ARTICLE INFO

Article history:
Received 5 September 2019
Received in revised form 19 December 2019
Accepted 19 December 2019
Available online 20 December 2019

Keywords:
Silicon quantum dots
DTNB
Fluorescence
Thiols
Cell imaging

ABSTRACT

An efficient and stable fluorescent sensor is described for the detection and imaging of thiols. It is making use of silicon quantum dots (SiQDs) which can be rapidly prepared. They were characterized by transmission electron microscopy, X-ray power diffraction, Fourier transform infrared spectroscopy, X-ray photoelectron spectrometry. The SiQDs have an absorption maximum at 300 nm and displayed blue-green fluorescence with excitation/emission maxima at 410/480 nm. A mixture of SiQDs and 5,5′-dithiobis-(2-nitrobenzoic acid) (DTNB) exhibits strong fluorescence emission which however is quenched within 30 s of incubation with thiols. This is assumed to be due to an inner filter effect caused by the reaction of DTNB and thiols. The following thiols were tested: cysteine, homocysteine, and glutathione. The sensor has a linear response in the 3–100 μM thiol concentration range, and the LODs are between 0.80 and 0.96 μM. The sensor displays low cytotoxicity and was applied to fluorescence imaging of MCF-7 cells and Hela cells where it demonstrated excellent biocompatibility.

1. Introduction

Thiols such as cysteine (Cys), homocysteine (Hcy), and glutathione (GSH) are widely distributed in tissues and cells. Thiols play crucial roles in many physiological processes such as maintenance of intra- and extracellular redox status, resistance against external harmful effects, stabilization of protein structures and function, intracellular signal transduction, gene regulation, increasing blood-brain barrier permeability, metabolism and detoxification [1,2]. Abnormal levels of thiols can lead to various kinds of health problems [1]. Small molecular thiols as effective biomarkers can provide diagnostic information for above diseases [3]. Therefore, the development of methods for quantitative analysis of thiols is of great significance.

Several methods have been reported for thiols detection including electrochemical technology [4], high performance liquid chromatography (HPLC) [5], fluorescence spectrometry [6], mass spectrometry [7] etc. Among them, fluorescent assay has attracted more attention due to its advantages of high sensitivity [6]. Various types of fluorescent probes have been utilized for chemical sensing such as fluorescent polymeric probes [8–12], core quantum dots [13,14], core-shell quantum dots [15,16], alloyed quantum dots [17,18] etc. However, most of current fluorescent sensors for thiols were complex in synthesis [19], slow in response [20], narrow in linear range [21], potential in toxicity [6] and not resistant to photobleaching, which limited their application in bioanalysis. For instance, Anamika et al. [6] detected L-cysteine and glutathione in water and urine with good sensitivity by using crystal violet-functionalized CdTe quantum dots, however, which may have potential heavy-metal toxicity. Kubilay et al. [22] and Yang et al. [23] successively fabricated Au-NPs (gold nanoparticles) based and NCQDs (nitrogen-doped carbon quantum dots) based sensors for thiols. Both assays utilized the selectivity of Ellman's reagent 5,5′-disulfide (2-nitrobenzoic acid) (DTNB) and the sensitivity of the fluorescence materials, and were successfully used to detect thiols in pharmaceutical samples and serum samples respectively, but neither can detect intracellular thiols due to the limitation of material properties. Hence, it is still necessary to prepare stable and biocompatible fluorescent materials for the detection of thiols in cell samples.

Studies have demonstrated that SiQDs had superior biocompatibility and the biodegradation products-silicic acid can be excreted through urine [24,25]. Besides, the photostability of SiQDs was usually better than that of ordinary organic dyes and most semiconductor nanomaterials [24,26]. For example, upon high-power UV irradiation, the fluorescence of fluorescein isothiocyanate was quickly quenched after 5 min, the fluorescence of CdTe QDs or CdSe/ZnS QDs was retained for 120 min, while the fluorescence of SiQDs maintained stable for 400 min [24]. Especially, the SiQDs with abundant amino terminals

* Corresponding author.
E-mail address: hongwang@whu.edu.cn (H. Wang).
[1] These authors contributed equally to this manuscript.

https://doi.org/10.1016/j.saa.2019.117972
1386-1425/

were supposed to have high fluorescence yields, good water-solubility and fast preparation methods [25]. Thus, they were widely used in bioimaging such as lysosome imaging [25], intracellular ROS (reactive oxygen species) imaging [27], and other cellular imaging [28]. However, the number of fluorescent sensors for thiols detection based on SiQDs has been very limited by now. Ma et al. [28] prepared a glutathione sensor based on SiQDs modified with MnO_2 nanosheets which was applied in bioimaging. However, it was susceptible to the interference of cell autofluorescence, and the cytotoxicity of the sensor was not neglectable due to the metal dopants. Therefore, it is necessary to develop a new metal-free fluorescent sensor with real biocompatibility and high efficiency for thiols detection.

Herein, we pretended a non-metal and super miniature blue-green fluorescent sensor (SiQDs-DTNB) for thiols by using SiQDs as fluorescent subjects and DTNB as thiols recognizing groups. Water-soluble SiQDs were synthesized using (3-aminopropyl)trimethoxysilane (APTMS) and glucose. The SiQDs-DTNB was formed by mixing DTNB with SiQDs solution. The SiQDs-DTNB exhibited good selectivity and sensitivity for thiols detection. The principle of this sensor is illustrated in Fig. 2. After incubation with thiols for only 30 s, an intense fluorescence quenching was appeared based on inner filter effect (IFE) between SiQDs and 5-thio-2-nitrobenzoic acid (TNBA, the reaction product of DTNB and thiols). Compared with previous reports, this assay avoided high-temperature processing [25], metal toxicity [6], long reaction time [20] and intricate equipment [5]. Especially, the SiQDs-DTNB was further used for cell imaging owing to the strong photostability and excellent biocompatibility.

2. Materials and methods

2.1. Reagents

DTNB, (3-aminopropyl)trimethoxysilane (APTMS), rhodamine B, N-ethylmaleimide (NEM), Cys, Hcy, GSH and other amino acids were supplied by Aladdin Reagent Co., Ltd. (Shanghai, China). Dimethylsulfoxide (DMSO), ascorbic acid (Vc), citric acid, glucose, NaCl, Na_2SO_4 and other salts were obtained from Sinopharm Chemical Reagent Co., Ltd. (Shanghai, China). 3-(4,5-dimethyl-2-thiazolyl)-2,5-diphenyltetrazolium bromide (MTT), Dulbecco's modified Eagle medium (DMEM), non-mycoplasma fetal bovine serum (FBS), penicillin-streptomycin solution and trypsin were purchased from Dingguo Changsheng Biotechnology Co., Ltd. (Beijing, China). All the chemicals above were of analytical grade. Ultrapure water (18.25 M Ω cm) was acquired by an ultrapure water manufacturing system (Ulupure, China) and used in the whole experiment process. Aqueous solutions applied for cellular imaging were filtered by 0.22 μm membrane (Jin Teng, China) before use.

2.2. Apparatus

The surface morphology of SiQDs was obtained by JEM2100 transmission electron microscopy (TEM) (JEOL Ltd., Japan). The hydrodynamic size distribution of SiQDs in water was performed at 25 °C on a Zetasizer Nano ZSP (Malvern. UK). The crystal structure of SiQDs was measured by Miniflex600 X-ray power diffraction (PXRD) (Rigaku, Japan). The functional groups on the surface of SiQDs were analyzed by iS10 Fourier transform infrared spectrophotometer (FTIR) (Thermo, America). The surface chemical composition of SiQDs was characterized by Escalab250Xi X-ray photoelectron spectrometry (XPS) (Thermo, America). The absorption spectra and fluorescence spectra (FL) were respectively recorded by UV-4802 UV–visible spectrophotometer (Unico, China) and RF-6000 fluorescence spectrometer (Shimadzu, Japan). The fluorescence lifetime decay curves were gained by a FLS1000 (Edinburgh, Britain). MTT assays were measured with Spark 10 M enzyme marker (Tecan, Switzerland). Fluorescence images were taken with 405 nm excitation by UltraVIEW VoX confocal microscope (PerkinElmer, America) at 60 x magnification. The wavelength of filter was 525 nm (bandwidth was 50 nm), the exposure time was 600 ms, and the power of excited light was 50.5%.

2.3. Synthesis of SiQDs

The SiQDs were synthesized according to the literatures [29] with some modification. 0.12 g of glucose and 3.75 mL of (3-aminopropyl) trimethoxysilane (APTMS) were dissolved in 12 mL of ultrapure water. To facilitate the reaction, 20 μL of 1 M NaOH was subsequently added and stirred for 30 min at 60 °C. After reaction, the solution was neutralized by HCl (6 M) and dialyzed (1 kDa MWCO) against ultrapure water for 24 h. The SiQDs were then freeze-dried and stored at 4 °C until further analysis.

2.4. Fluorescence detection of thiols

The detection of thiols was performed in phosphate buffered saline (PBS, 0.01 M, pH 7.4) at 25 °C. Firstly, 0.5 mL of SiQDs solution ($0.5\ g \cdot L^{-1}$) was added to the DTNB solution (0.4 mg of DTNB dissolved in 4 mL of PBS) and shaken thoroughly to form the SiQDs-DTNB solution. Then, 0.5 mL of different concentrations of thiols or blank was added to the solution above. The mixture was shaken thoroughly and incubated for 30 s at 25 °C. After that, the fluorescence emission spectra were recorded under the excitation wavelength at 410 nm. The scanning was down between 420 nm and 600 nm. The excitation and emission slit widths were 5 and 10 nm, respectively.

2.5. Cell culture, fluorescence imaging and cytotoxicity test

2.5.1. Cell culture and fluorescence imaging

MCF-7 cells and Hela cells were cultured in Dulbecco's modified Eagle medium (DMEM) complemented by 10% (v/v) FBS and 1% (v/v) penicillin-streptomycin solution at 37 °C in a 5% CO_2 and 95% humidity incubator. Before fluorescence imaging, cells were seeded into the culture dishes and cultured with SiQDs ($1.4\ g \cdot L^{-1}$) for 4 h. Subsequently, DTNB (0.2 mM) was added and incubated for 30 min. The cells pretreated with NEM for 15 min acted as a control. The cells were washed three times with PBS to remove excess compound before analysis.

2.5.2. Cytotoxicity test

MCF-7 cells and Hela cells ($1 \times 10^5\ cells \cdot mL^{-1}$) were grown on 96-well plates for 24 h, then incubated in the solution of SiQDs (0, 0.2, 0.4, 0.6, 0.8, 1.0, 1.2, $1.4\ g \cdot L^{-1}$, respectively) with the absence or presence of DTNB (0.2 mM) for 24 h at 37 °C in a 5% CO_2 atmosphere. After discarding the culture medium, 0.2 mL of MTT ($0.5\ g \cdot L^{-1}$) were added to each well. About 4 h later, the MTT was replaced by 0.2 mL of DMSO in each well. Absorbance value of each well was measured at 570 nm. The cell viability was estimated as a ratio against the mean absorbance of untreated cells.

3. Results and discussion

3.1. Choice of materials

Appropriate fluorophore and quencher are crucial to improve the detection efficiency of fluorescence “turn off” sensor. SiQDs have been widely used in cell imaging due to their good water-solubility, photostability and biocompatibility [27]. Additionally, SiQDs has a lot of amino groups on the surface, which is beneficial to construct stable mixture with DTNB. On the other hand, thiols can reduce DTNB into TNBA. The absorption spectrum of TNBA overlaps with the fluorescence excitation spectrum of SiQDs, which can trigger the IFE process and quench the fluorescence of SiQDs effectively. Moreover, the large specific surface area of SiQDs makes SiQDs easier to contact with DTNB which further improves the sensitivity of the assay. Therefore, inspired

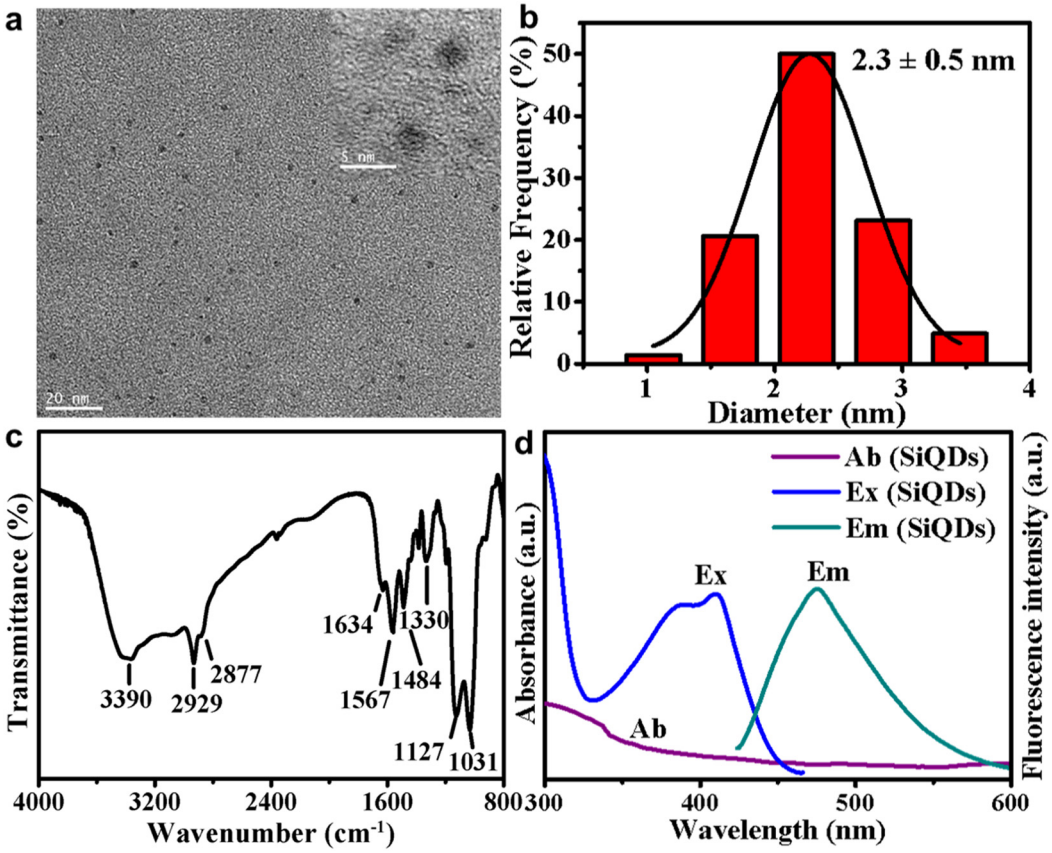

Fig. 1. (a) TEM images of SiQDs. Inset is the high-resolution TEM. (b) Particle size statistics and Gauss fit of SiQDs. (c) FTIR of SiQDs. (d) The absorption (Ab), excitation (Ex) and emission (Em) spectra of SiQDs. (λ_{ex} = 410 nm, λ_{em} = 480 nm).

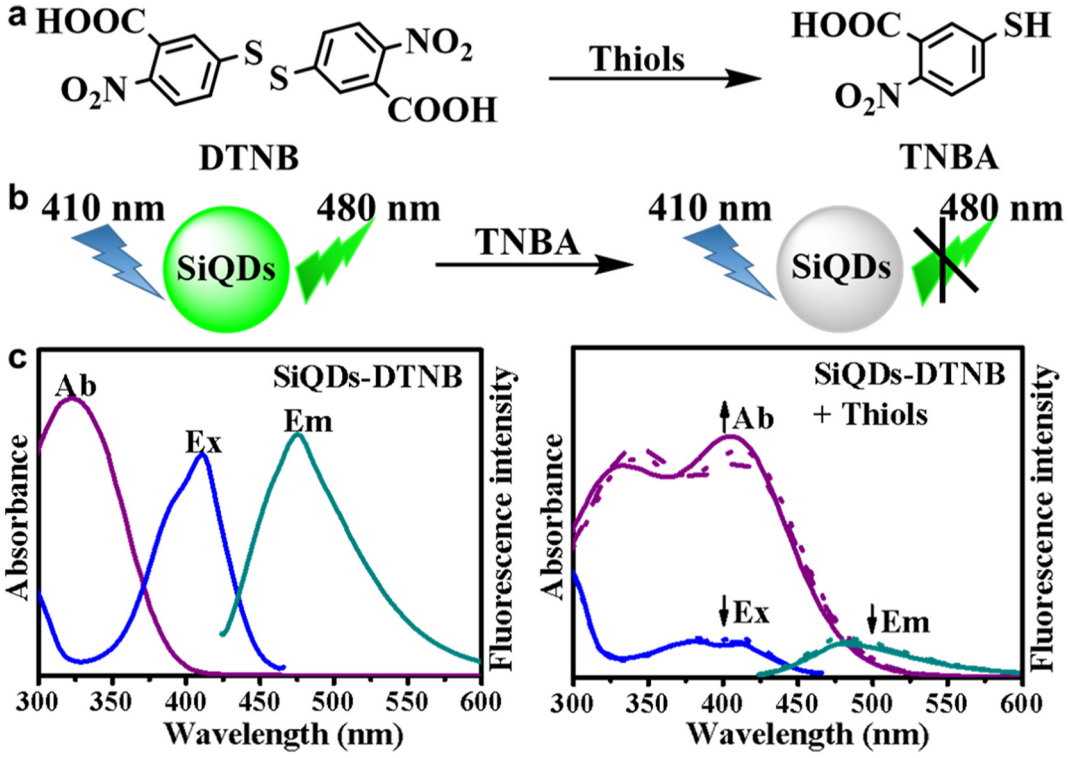

Fig. 2. Schematic illustration for thiols detection based on SiQDs-DTNB (Cys, solid line; Hcy, dash line; GSH, dot line).

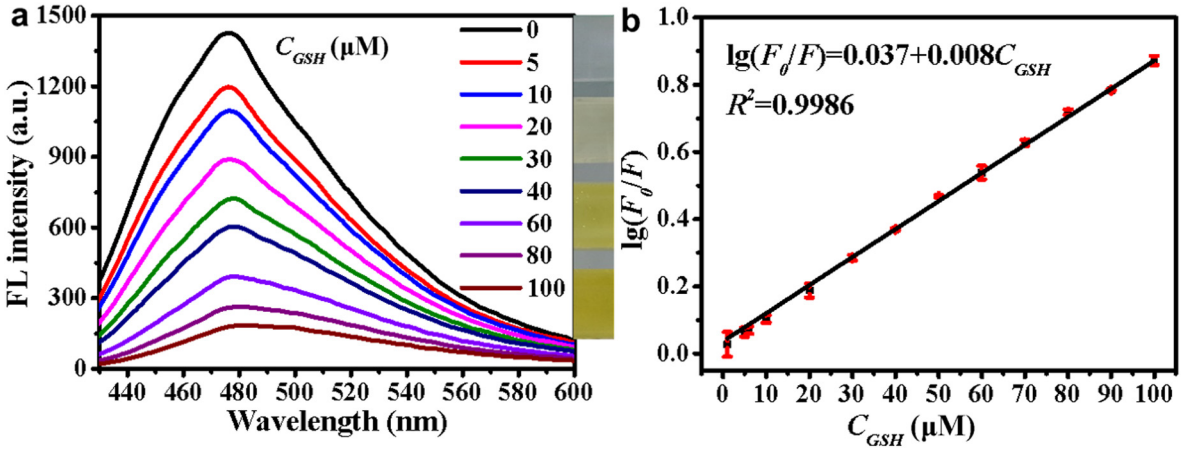

Fig. 3. (a) Fluorescence spectra of SiQDs-DTNB versus different concentrations of GSH. Inset indicates that the solution changes from colorless to yellow gradually with the increase of thiols concentration. (b) log (F_0/F) of SiQDs-DTNB as a function of the concentrations of GSH. (λ_{ex} = 410 nm, λ_{em} = 480 nm).

by combing the SiQDs with DTNB, and redox reaction between DTNB and thiols, a sensitive fluorometric detection for thiols was designed.

3.2. Characterization of SiQDs

Fig. 1a demonstrates the TEM of spherical particles with good monodispersity. The size distribution (Fig. 1b) indicated that the average diameter of the SiQDs was 2.3 ± 0.5 nm. The average hydrodynamic size of SiQDs in water measured by dynamic light scattering was about 13.4 nm (Fig. S1). XRD analysis confirmed that the SiQDs was in amorphous phase (Fig. S2f) [30] which were in accordance with the TEM images (Fig. 1a).

FTIR was carried out to investigate the surface functional groups of the SiQDs. As shown in Fig. 1c, the broad absorption at 3390 cm^{-1} was pertained to stretching vibrations of O—H and N—H. The absorption bands at 1634 cm^{-1} and 1567 cm^{-1} were originated from in-plane bending vibrations of N—H. The absorption peaks related to the N—H in the FTIR spectrum elucidated that the SiQDs contained a lot of amino groups on the surface [29]. Furthermore, the strong absorption at 2929 cm^{-1} and 2877 cm^{-1} was attributed to stretching vibrations of CH_3— and —CH_2—. The absorption peak at 1484 cm^{-1} corresponded to bending vibrations of C—H. The absorption peak at 1330 cm^{-1} belonged to stretching vibrations of C—N. The absorption bands at 1127 cm^{-1} and 1031 cm^{-1} were assigned to stretching vibrations of Si—O—Si and Si—O—C [31], indicating that Si—O was rich in the SiQDs.

The surface composition and element of the SiQDs was further confirmed by the XPS spectra (Fig. S2a–e). As revealed in the full-scan XPS spectra (Fig. S2a), five distinct peaks at 102.3, 152.9, 284.8, 398.9, and 531.8 eV were respectively corresponded to Si 2p, Si 2s, C 1s, N 1s, and O 1s [28]. Four peaks in the C 1s XPS spectrum (Fig. S2b) demonstrated the presence of C—Si (248.3 eV), C—C (284.5 eV), C—N (285.1 eV), C—O (285.7 eV) [32]. The N 1s XPS spectrum (Fig. S2c) displayed three peaks which were assigned to Si—N—Si (398.4 eV), C—N—C (398.9 eV), Si—N—O (399.6 eV), respectively [30]. The O—Si bond signal appeared at 531.3 eV and 531.8 eV in the O 1s XPS spectrum (Fig. S2d), and the C—O bond was detected at 532.1 eV [32]. The Si 2p XPS spectrum (Fig. S2e) exhibited three peaks which were ascribed to Si—C (101.8 eV), Si—N (102.2 eV), Si—O (102.7 eV) [29]. Those results of XPS analysis were consistent with the FTIR results (Fig. 1c).

Furthermore, the absorption (Ab), excitation (Ex) and emission (Em) spectra of SiQDs are shown in Fig. 1d. The SiQDs exhibited a broad absorption for the wavelength region below 450 nm and the fluorescence emission peak appeared at 480 nm when excited at 410 nm. The fluorescence quantum yield (QY) of SiQDs was determined to be 0.33 according to reported procedure [23] (Fig. S3 and Table S1). Such a high QY demonstrated that the SiQDs has an excellent fluorescence in aqueous solutions or organic solvents.

3.3. Principle for the analysis of thiols

As illustrated in Fig. 2, the assay for thiols detection was designed according to inner filter effect (IFE) quenching mechanism of SiQDs. And the mechanism was verified by UV–vis spectra and fluorescence spectra (Fig. 2b). It has been reported that Ellman's reagent DTNB can be reduced to TNBA by splitting the disulfide bonds upon the reaction with thiols [4] (Fig. 2a). TNBA is an intense yellow chromophore at pH 7.27 and has a strong absorbance at 412 nm with a molar extinction coefficient of 1.415 × 10^4 L mol^{-1} cm^{-1} [22]. IFE occurs when the absorption spectrum of TNBA overlapped with the excitation spectrum of SiQDs (λ_{ex} = 410 nm) (Fig. 2b). As shown in Fig. 2c, an absorption peak appeared at 410 nm upon addition of thiols (0.1 mM), leading to a

Table 1
Comparison of methods based on different fluorescent materials for thiols detection.

Method	Linear range (μM)			LOD (nM)			Analysis time	Reference
	Cys	HCy	GSH	Cys	HCy	GSH		
Maleimide-based	0.1–1.2	0–0.6	0.1–0.6	135	144	88.5	2 h	[20]
Binaphthalene-maleimide based	0–30	0–30	0–30	42.6	16.7	52.8	8 min	[19]
GQDs-Hg^{2+} system	0–0.13	0–0.1	0–0.05	2.5	5	5	15 min	[21]
BSA-silver nanoclusters	2–90	2–120	10–80	810	1000	1100	30 s	[1]
CV-CdTe quantum dots	0.02–40	Not given	0.02–50	10.5	Not given	8.2	5 min	[6]
MnO_2-CQDs	Not given	Not given	0–200	Not given	Not given	10	5 min	[34]
Tyr-CDs	1–50	5–50	0.1–5	120	3500	31	15 min	[35]
SiQDs-DTNB system	3–100	3–100	3–100	962	834	803	30 s	Our work

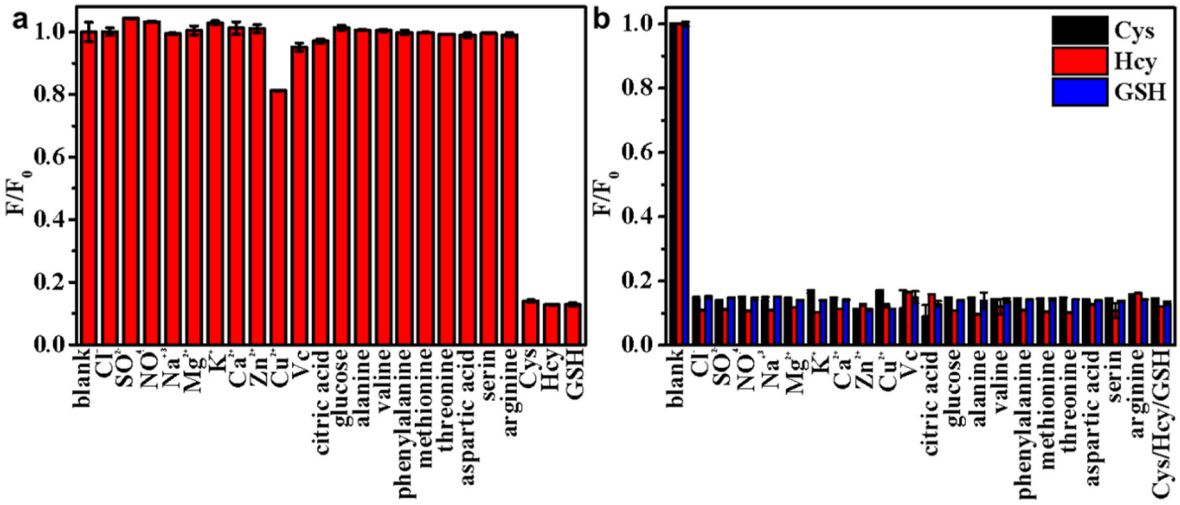

Fig. 4. (a) Fluorescence response (F/F_0) of the SiQDs-DTNB to interferences and thiols. (b) Fluorescence response (F/F_0) of the SiQDs-DTNB to the mixture of interferences and thiols. ($\lambda_{ex} = 410$ nm, $\lambda_{em} = 480$ nm).

fluorescence quenching of SiQDs-DTNB. The phenomenon above implied that this assay based on IFE was effective for thiols detection.

In addition, to explore the possibility of dynamic quenching effect (DQE) and stative quenching effect (SQE), the Stern-Volmer equation was investigated:

$$\frac{F_0}{F} = 1 + K_{SV}[Q]$$

where, F_0 and F refer to the steady-state fluorescence intensity in the absence and presence of thiols, respectively; K_{SV} is the Stern-Volmer constant and [Q] is the concentration of thiols, respectively. As displayed in Fig. S4, there was no linear relationship between the value of F_0/F and the concentration of thiols, which suggested that the mechanism of DQE and SQE were negligible [30]. Besides, the steady state fluorescence and time resolved fluorescence experiment has been performed and the result was shown in Fig. S5, the changes of fluorescence lifetime of SiQDs-DTNB after the addition of thiols were negligible (<0.3 ns).

Based on the above discussion, the quenching process is mainly arisen from the IFE mechanism between SiQDs-DTNB and thiols.

3.4. Optimization of experimental conditions

To optimize the performance of the assay, the following parameters were optimized: reaction time, reaction temperature and sample pH value. The fluorescence quenching rapidly reaching the platforms in about 30 s upon addition of thiols into the SiQDs-DTNB solution (Fig. S6a). With the increase of temperature, the fluorescence intensity of SiQDs and SiQDs-DTNB can decrease (Fig. S6b). Furthermore, the fluorescence intensity of SiQDs-DTNB was highest under pH 7 (Fig. S6c). Considering the potential application in biological systems, the optimum experimental conditions were selected as reaction time of 30 s, reaction temperature of 25 °C and sample pH value of 7.4 for further study.

Table 2
The analysis of thiols in the fetal bovine serum samples ($n = 3$).

Samples	Amount added (μM)	Amount found (μM)	Recovery (%)	RSD (%)
Cys	10	9.51	95.1	1.1
	20	19.50	97.5	4.2
	40	41.06	102.6	1.8
Hcy	10	10.36	103.6	2.7
	20	20.98	104.9	1.0
	40	41.89	104.7	0.3
GSH	10	10.19	101.9	1.3
	20	19.86	99.3	0.2
	40	40.42	101.1	4.2

3.5. Optical responses to thiols

Under the optimal conditions discussed above, analytical performance of the sensor was investigated. The FL intensity of SiQDs-DTNB gradually decreased upon the addition of GSH (Fig. 3a), Cys (Fig. S7a) and Hcy (Fig. S7c) with increased concentration. The color variations of the solution in the presence of various concentration of thiols were observed visually (inset in Fig. 3a), which provided a visual approach to rough detection of thiols.

Besides, the quenching efficiency [$\log(F_0/F)$] was proportional to the concentration of thiols, which was similar with previous work in other reports [30] (F_0 and F were the FL intensity of SiQDs-DTNB in the absence and presence of thiols, respectively). The linear range of the SiQDs-DTNB system for GSH, Cys and Hcy were found to be 3–100 μM ($Y = 0.037 + 0.008X$, inset in Fig. 3b), 3–100 μM ($Y = 0.023 + 0.009X$, inset in Fig. S7b) and 3–100 μM ($Y = 0.008 + 0.008X$, inset in Fig. S7d), respectively. The detection limits for GSH, Cys and Hcy were similar and respectively determined to be 0.80 μM, 0.96 μM and 0.83 μM (Fig. S8 and Table S2), which were much lower than the normal concentration of thiols in biosystem (1–10 mM of GSH and 30–200 μM of Cys in cells [33], 5–15 μM of Hcy in plasma [2]).

Furthermore, the linear response range and the detection limit discussed above were comparable to those of previous fluorescent materials for thiols detection (Table 1). Additionally, the sensor exhibited relatively swifter response than most sensors before, which enhanced the effectiveness of thiols detection (Table 1). As a consequence, the sensor displayed a reliable and effective method for thiols detection.

3.6. Effect of potential interfering substances

The impact of some inorganic ions and organic molecules was investigated under the optimal detection condition. Cl^-, SO_4^{2-}, NO_3^-, Na^+, Mg^{2+}, K^+, Ca^{2+}, Zn^{2+}, Cu^{2+}, Vc (ascorbic acid), citric acid, glucose, alanine, valine, phenylalanine, methionine, threonine, aspartic acid, serine and arginine were selected as potential interfering species. The concentration of Zn^{2+} was 0.5 mM, Cu^{2+} was 0.03 mM, and other interferences were 1 mM. The concentrations of Cys, Hcy and GSH were all 0.1 mM.

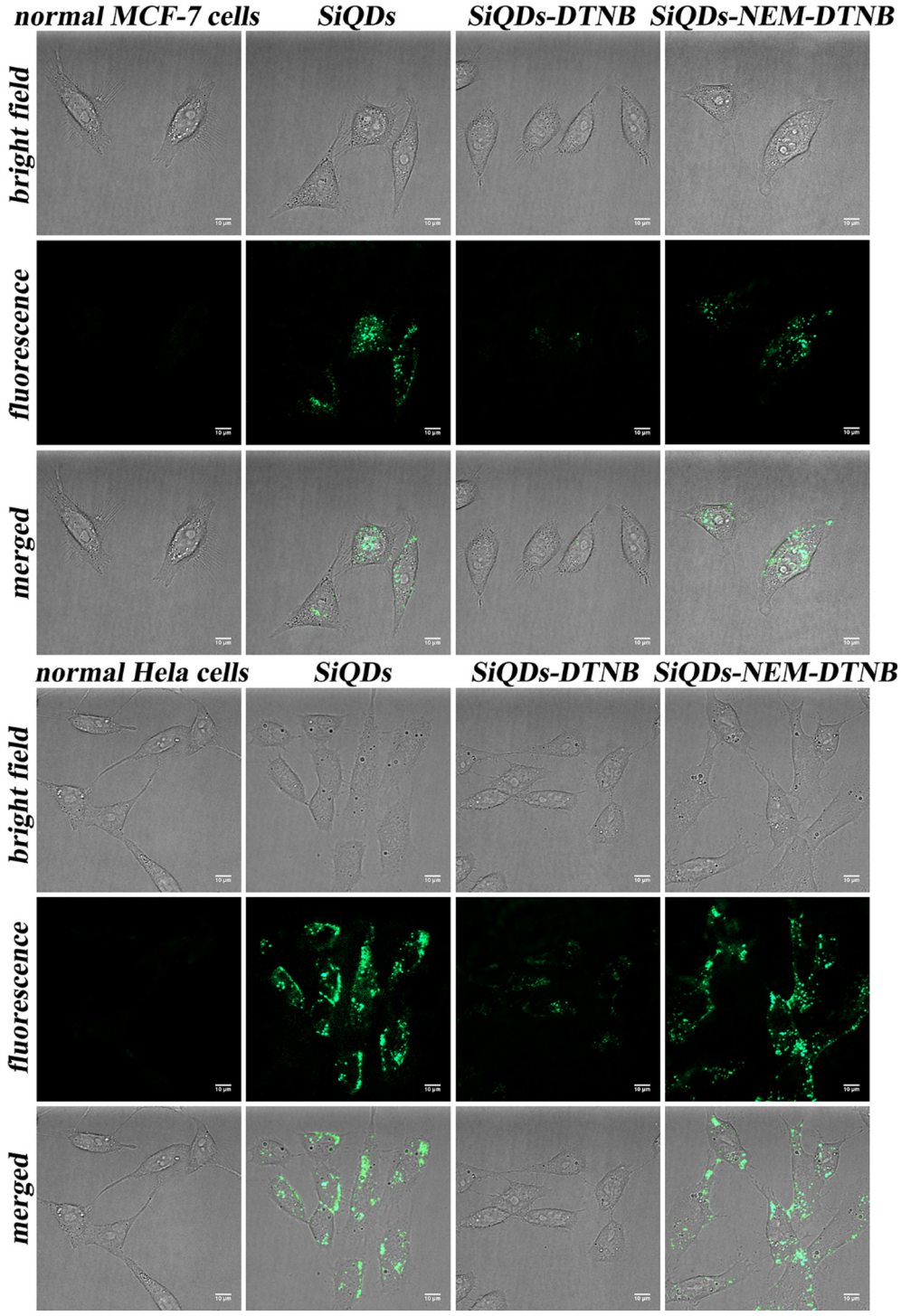

Fig. 5. Confocal microscopy images of MCF-7 cells and Hela cells under bright field, fluorescence, and merged. The designation "SiQDs" represents cells incubated with SiQDs ($1.4\ g \cdot L^{-1}$) for 4 h. The designation "SiQDs-DTNB" represents cells further incubated with DTNB (0.2 mM) for 30 min. The designation "SiQDs-NEM-DTNB" represents cells firstly incubated with SiQDs for 4 h, then treated with NEM (0.5 mM) for 15 min, finally incubated with DTNB for 30 min.

As shown in Fig. 4a, the effect of other interferences on fluorescence response of SiQDs-DTNB was <5% except Cu^{2+} (20%). In an oxygen atmosphere, Cu^{2+} catalyzes the oxidation of Cys to form cystine and H_2O_2 [36]. This may disturb the assay. Nevertheless, the concentration of intracellular free copper ions is usually lower than 1 pM [37]. Such trace amounts of Cu^{2+} do not cause much influence. Negligible influence on fluorescence intensity of SiQDs-DTNB was observed after addition of a mixture including thiols and these potential interfering substances (Fig. 4b). Overall, SiQDs-DTNB displayed an excellent selectivity towards thiols over other interferences.

3.7. Cytotoxicity, photostability and practicability

The cytotoxicity of SiQDs and SiQDs-DTNB was evaluated by a standard MTT assay [38–42]. As shown in Fig. S9a, the cell viability for MCF-7 cells was still approximate to 80% after 24 h of exposure to SiQDs or

SiQDs-DTNB at concentrations below 1.4 $g \cdot L^{-1}$. Similarly, SiQDs and SiQDs-DTNB showed very low toxicity for Hela cells at the same conditions (Fig. S9b).

For photostability experiment, the FL intensity of SiQDs and SiQDs-DTNB remained higher than 90% of the initial intensity after continuous irradiation with 90 W incandescent lamp for 12 h (Fig. S6d). The results indicated that the sensor had good photostability in PBS (0.01 M, pH 7.4) and adapted for long term detection.

The detection of thiols in FBS samples was preformed to evaluate the practicability of the assay. The FBS sample was diluted 300-fold with PBS (0.01 M, pH 7.4) and directly used for assay. The recovery of the samples ranged from 95.1% to 104.9% with the relative standard Deviations (RSDs) of 0.2–4.2% (Table 2). Therefore, the assay offers a feasible alternative for thiols detection in real samples.

Additionally, the bio-imaging nature of the sensor was examined in the MCF-7 cells and Hela cells (Fig. 5). Compared with normal cells, the cells cultured with SiQDs for 4 h exhibited obvious fluorescence signal, indicating that SiQDs entered cells and mainly distributed in the cytoplasm [43–45]. The fluorescence intensity didn't change much with incubating time prolonging (Fig. S10). The fluorescence signal was significantly reduced after further 30 min incubation with DTNB (0.2 mM). In comparison, the cells pretreated for 15 min with a scavenger of thiols (N-ethylmaleimide, NEM, 0.5 mM) still maintained strong fluorescence signal. The study in vitro imaging demonstrated that the sensor can react with thiols in cells without noticeable cytotoxicity [46–48].

4. Conclusion

In summary, a non-metal sensor (SiQDs-DTNB) based on IFE mechanism was designed for the detection of thiols. The sensor exhibited similar behavior in fluorescence response for Cys, Hcy and GSH with the analysis time as short as 30 s. Moreover, SiQDs-DTNB was stable and effective enough to be used for detection of thiols in serum samples as well as living cells. Therefore, the assay provided a biocompatible nano-platform for thiols detection, laying a foundation for the biomedical analysis of silicon sensor in the future.

CRediT authorship contribution statement

Bo-Hui Huang: Conceptualization, Methodology, Writing - original draft. **San-San Shen:** Data curation, Formal analysis, Software. **Na Wei:** Visualization, Investigation, Validation. **Xiao-Feng Guo:** Writing - review & editing, Project administration. **Hong Wang:** Resources, Supervision, Funding acquisition.

Declaration of competing interest

The authors declare that they have no known competing financial interests or personal relationships that could have appeared to influence the work reported in this paper.

Acknowledgment

This work was supported by the National Natural Science Foundation of China (Nos. 20835004, 31670370 and 21777126, Beijing, China).

Appendix A. Supplementary data

Supplementary data to this article can be found online at https://doi.org/10.1016/j.saa.2019.117972.

References

[1] Z. Chen, D.T. Lu, Z.W. Cai, C. Dong, S.M. Shuang, Bovine serum albumin-confined silver nanoclusters as fluorometric probe for detection of biothiols, Luminescence 29 (2014) 722–727, https://doi.org/10.1002/bio.2613.

[2] H. Skovierova, E. Vidomanova, S. Mahmood, J. Sopkova, A. Drgova, T. Cervenova, E. Halasova, J. Lehotsky, The molecular and cellular effect of homocysteine metabolism imbalance on human health, Int. J. Mol. Sci. 17 (2016) 1733, https://doi.org/10.3390/ijms17101733.

[3] C.X. Yin, F.J. Huo, J.J. Zhang, R. Martinez-Manez, Y.T. Yang, H.G. Lv, S.D. Li, Thiol-addition reactions and their applications in thiol recognition, Chem. Soc. Rev. 42 (2013) 6032–6059, https://doi.org/10.1039/c3cs60055f.

[4] O. Nekrassova, P.C. White, S. Threlfell, G. Hignett, A.J. Wain, N.S. Lawrence, J. Davis, R.G. Compton, An electrochemical adaptation of Ellman's test, Analyst 127 (2002) 797–802, https://doi.org/10.1039/b202780c.

[5] A. Kaminska, P. Olejarz, K. Borowczyk, R. Glowacki, G. Chwatko, Simultaneous determination of total homocysteine, cysteine, glutathione, and N-acetylcysteine in brain homogenates by HPLC, J. Sep. Sci. 41 (2018) 3241–3249, https://doi.org/10.1002/jssc.201800381.

[6] Z. Sheng, L.G. Chen, Switch-on fluorescent strategy based on crystal violet-functionalized CdTe quantum dots for detecting L-cysteine and glutathione in water and urine, Anal. Bioanal. Chem. 409 (2017) 6081–6090, https://doi.org/10.1007/s00216-017-0541-1.

[7] X.M. Yuan, Y.L. Lu, C. Xiao, J.M. Zhu, W. Zhang, C. Yu, S.J. Li, Application of a micro plasma collection card for the detection of homocysteine by liquid chromatography with tandem mass spectrometry, J. Sep. Sci. 41 (2018) 4167–4176, https://doi.org/10.1002/jssc.201800579.

[8] J. Liu, J.W.Y. Lam, B.Z. Tang, Acetylenic polymers: syntheses, structures, and functions, Chem. Rev. 109 (2009) 5799–5867.

[9] X. Zhang, K. Wang, M. Liu, X. Zhang, L. Tao, Y. Chen, Y. Wei, Polymeric AIE-based nanoprobes for biomedical applications: recent advances and perspectives, Nanoscale 7 (2015) 11486–11508, https://doi.org/10.1039/c5nr01444a.

[10] Z. Long, L. Mao, M. Liu, Q. Wan, Y. Wan, X. Zhang, Y. Wei, Marrying multicomponent reactions and aggregation-induced emission (AIE): new directions for fluorescent nanoprobes, Polym. Chem. 8 (2017) 5644–5654, https://doi.org/10.1039/c7py00979h.

[11] Q. Wan, Q. Huang, M. Liu, D. Xu, H. Huang, X. Zhang, Y. Wei, Aggregation-induced emission active luminescent polymeric nanoparticles: non-covalent fabrication methodologies and biomedical applications, Appl. Mater. Today 9 (2017) 145–160, https://doi.org/10.1016/j.apmt.2017.06.004.

[12] L. Mao, Y. Liu, S. Yang, Y. Li, X. Zhang, Y. Wei, Recent advances and progress of fluorescent bio-/chemosensors based on aggregation-induced emission molecules, Dyes Pigments 162 (2019) 611–623, https://doi.org/10.1016/j.dyepig.2018.10.045.

[13] E. Zenkevich, A. Shulga, F. Cichos, E. Petrov, T. Blaudeck, C. von Borczyskowski, Nanoassemblies designed from semiconductor quantum dots and molecular arrays, J. Phys. Chem. B 109 (2005) 8679–8692.

[14] S. D'Souza, E. Antunes, C. Litwinski, T. Nyokong, Photophysical behavior of zinc monoaminophthalocyanines linked to mercaptopropionic acid-capped CdTe quantum dots, J. Photochem. Photobiol. A Chem. 220 (2011) 11–19, https://doi.org/10.1016/j.jphotochem.2011.03.005.

[15] I.V. Martynenko, A.O. Orlova, V.G. Maslov, A.V. Baranov, A.V. Fedorov, M. Artemyev, Energy transfer in complexes of water-soluble quantum dots and chlorin e6 molecules in different environments, Beilstein J Nanotechnol 4 (2013) 895–902, https://doi.org/10.3762/bjnano.4.101.

[16] A. Ray, A. De, S. Bhattacharya, Study of energy transfer phenomenon between quantum dots and zinc porphyrin in solution, J. Mol. Liq. 246 (2017) 17–24, https://doi.org/10.1016/j.molliq.2017.08.090.

[17] A. Ray, S. Bhattacharya, A. Bauri, Exhibition of Förster resonance energy transfer from CdSe/ZnS quantum dots to zinc porphyrazine studied in solution, J. Mol. Liq. 276 (2019) 770–778, https://doi.org/10.1016/j.molliq.2018.11.141.

[18] A. Ray, A. Bauri, S. Bhattacharya, Study of chemical physics on energy transfer phenomenon between quantum dots and a designed diporphyrin in solution, J. Mol. Liq. 263 (2018) 64–71, https://doi.org/10.1016/j.molliq.2018.04.035.

[19] Y. Zhang, F. Huo, C. Yin, Y. Yue, J. Hao, J. Chao, D. Liu, An off–on fluorescent probe based on maleimide for detecting thiols and its application for bioimaging, Sens. Actuators B Chem. 207 (2015) 59–65, https://doi.org/10.1016/j.snb.2014.09.091.

[20] L. Qu, C. Yin, F. Huo, J. Li, J. Chao, Y. Zhang, A maleimide-based thiol fluorescent probe and its application for bioimaging, Sens. Actuators B Chem. 195 (2014) 246–251, https://doi.org/10.1016/j.snb.2014.01.026.

[21] Z.Z. Wu, W.Y. Li, J. Chen, C. Yu, A graphene quantum dot-based method for the highly sensitive and selective fluorescence turn on detection of biothiols, Talanta 119 (2014) 538–543, https://doi.org/10.1016/j.talanta.2013.11.065.

[22] K. Güçlü, M. Özyürek, N. Güngör, S. Baki, R. Apak, Selective optical sensing of biothiols with Ellman's reagent: 5,5′-dithio-bis(2-nitrobenzoic acid)-modified gold nanoparticles, Anal. Chim. Acta 794 (2013) 90–98, https://doi.org/10.1016/j.aca.2013.07.041.

[23] J.S. Yang, H.X. Wu, P. Yang, C.J. Hou, D.Q. Huo, A high performance N-doped carbon quantum dots/5,5′-dithiobis-(2-nitrobenzoic acid) fluorescent sensor for biothiols detection, Sens. Actuators B Chem. 255 (2018) 3179–3186, https://doi.org/10.1016/j.snb.2017.09.143.

[24] H.Y. Wang, Y. He, Recent advances in silicon nanomaterial-based fluorescent sensors, Sensors 17 (2017) 268, https://doi.org/10.3390/s17020268.

[25] Y. Zhang, S. Guo, S. Cheng, X. Ji, Z. He, Label-free silicon nanodots featured ratiometric fluorescent aptasensor for lysosomal imaging and pH measurement, Biosens. Bioelectron. 94 (2017) 478–484, https://doi.org/10.1016/j.bios.2017.03.041.

[26] Z. Zhou, J.P. Gu, Y.Z. Chen, X.X. Zhang, H.X. Wu, X.G. Qiao, Europium functionalized silicon quantum dots nanomaterials for ratiometric fluorescence detection of Bacillus anthrax biomarker, Spectrochim. Acta Part A-Molecular Biomol. Spectrosc. 212 (2019) 88–93, https://doi.org/10.1016/j.saa.2018.12.036.

[27] Q.Q. Zhao, R. Zhang, D.X. Ye, S. Zhang, H. Chen, J.L. Kong, Ratiometric fluorescent silicon quantum dots-Ce6 complex probe for the live cell imaging of highly reactive

oxygen species, ACS Appl. Mater. Interfaces 9 (2017) 2052–2058, https://doi.org/10.1021/acsami.6b12047.
[28] H. Ma, X.R. Li, X.Y. Liu, M. Deng, X.D. Wang, A. Iqbal, W.S. Liu, W.W. Qin, Fluorescent glutathione probe based on MnO_2-Si quantum dots nanocomposite directly used for intracellular glutathione imaging, Sens. Actuators B Chem. 255 (2018) 1687–1693, https://doi.org/10.1016/j.snb.2017.08.170.
[29] L.M.T. Phan, S.H. Baek, T.P. Nguyen, K.Y. Park, S. Ha, R. Rafique, S.K. Kailasa, T.J. Park, Synthesis of fluorescent silicon quantum dots for ultra-rapid and selective sensing of Cr(VI) ion and biomonitoring of cancer cells, Mater. Sci. Eng. C-Materials Biol. Appl. 93 (2018) 429–436, https://doi.org/10.1016/j.msec.2018.08.024.
[30] Y. Han, Y. Chen, J. Liu, X. Niu, Y. Ma, S. Ma, X. Chen, Room-temperature synthesis of yellow-emitting fluorescent silicon nanoparticles for sensitive and selective determination of crystal violet in fish tissues, Sens. Actuators B Chem. 263 (2018) 508–516, https://doi.org/10.1016/j.snb.2018.02.163.
[31] L.Q. Du, Z.P. Li, J.L. Yao, G.M. Wen, C. Dong, H. Li, Enzyme free glucose sensing by amino-functionalized silicon quantum dot, Spectrochim. Acta Part A-Molecular Biomol. Spectrosc. Biomol. Spectrosc. 216 (2019) 303–309, https://doi.org/10.1016/j.saa.2019.03.071.
[32] Y.N. Liu, Q.Z. Wang, S.W. Guo, P. Jia, Y.H. Shui, S.Y. Yao, C. Huang, M. Zhang, L. Wang, Highly selective and sensitive fluorescence detection of hydroquinone using novel silicon quantum dots, Sens. Actuators B Chem. 275 (2018) 415–421, https://doi.org/10.1016/j.snb.2018.08.073.
[33] Y. Li, W. Liu, P. Zhang, H. Zhang, J. Wu, J. Ge, P. Wang, A fluorescent probe for the efficient discrimination of Cys, Hcy and GSH based on different cascade reactions, Biosens. Bioelectron. 90 (2017) 117–124, https://doi.org/10.1016/j.bios.2016.11.021.
[34] D.G. He, X.X. Yang, X.X. He, K.M. Wang, X. Yang, X. He, Z. Zou, A sensitive turn-on fluorescent probe for intracellular imaging of glutathione using single-layer MnO_2 nanosheet-quenched fluorescent carbon quantum dots, Chem. Commun. 51 (2015) 14764–14767, https://doi.org/10.1039/c5cc05416h.
[35] H.S. Zhu, E.K. Wang, J. Li, J. Wang, L-tyrosine methyl ester-stabilized carbon dots as fluorescent probes for the assays of biothiols, Anal. Chim. Acta 1006 (2018) 83–89, https://doi.org/10.1016/j.aca.2017.12.014.
[36] X.G. Chen, Q.J. Lu, D. Liu, C.Y. Wu, M.L. Liu, H.T. Li, Y.Y. Zhang, S.Z. Yao, Highly sensitive and selective determination of copper(II) based on a dual catalytic effect and by using silicon nanoparticles as a fluorescent probe, Microchim. Acta 185 (2018) 188, https://doi.org/10.1007/s00604-018-2720-y.
[37] F.B. Yu, W.S. Zhang, P. Li, Y.L. Xing, L.L. Tong, J.P. Ma, B. Tang, Cu(2+)-selective naked-eye and fluorescent probe: its crystal structure and application in bioimaging, Analyst 134 (2009) 1826–1833, https://doi.org/10.1039/b823360h.
[38] H. Huang, M. Liu, R. Jiang, J. Chen, L. Mao, Y. Wen, J. Tian, N. Zhou, X. Zhang, Y. Wei, Facile modification of nanodiamonds with hyperbranched polymers based on supramolecular chemistry and their potential for drug delivery, J. Colloid Interface Sci. 513 (2018) 198–204, https://doi.org/10.1016/j.jcis.2017.11.009.
[39] H. Huang, M. Liu, Q. Wan, R. Jiang, D. Xu, Q. Huang, Y. Wen, F. Deng, X. Zhang, Y. Wei, Facile fabrication of luminescent hyaluronic acid with aggregation-induced emission through formation of dynamic bonds and their theranostic applications, Mater. Sci. Eng. C Mater. Biol. Appl. 91 (2018) 201–207, https://doi.org/10.1016/j.msec.2018.05.015.
[40] R. Jiang, M. Liu, T. Chen, H. Huang, Q. Huang, J. Tian, Y. Wen, Q. Cao, X. Zhang, Y. Wei, Facile construction and biological imaging of cross-linked fluorescent organic nanoparticles with aggregation-induced emission feature through a catalyst-free azide-alkyne click reaction, Dyes Pigments 148 (2018) 52–60, https://doi.org/10.1016/j.dyepig.2017.09.005.
[41] R. Jiang, M. Liu, H. Huang, L. Mao, Q. Huang, Y. Wen, Q.Y. Cao, J. Tian, X. Zhang, Y. Wei, Facile fabrication of organic dyed polymer nanoparticles with aggregation-induced emission using an ultrasound-assisted multicomponent reaction and their biological imaging, J. Colloid Interface Sci. 519 (2018) 137–144, https://doi.org/10.1016/j.jcis.2018.01.084.
[42] L. Huang, S.J. Yang, J.Y. Chen, J.W. Tian, Q. Huang, H.Y. Huang, Y.Q. Wen, F.J. Deng, X.Y. Zhang, Y. Wei, A facile surface modification strategy for fabrication of fluorescent silica nanoparticles with the aggregation-induced emission dye through surface-initiated cationic ring opening polymerization, Mater. Sci. Eng. C-Materials Biol. Appl. 94 (2019) 270–278, https://doi.org/10.1016/j.msec.2018.09.042.
[43] X. Zhang, X. Zhang, B. Yang, M. Liu, W. Liu, Y. Chen, Y. Wei, Fabrication of aggregation induced emission dye-based fluorescent organic nanoparticles via emulsion polymerization and their cell imaging applications, Polym. Chem. 5 (2014) 399–404, https://doi.org/10.1039/c3py00984j.
[44] X. Zhang, X. Zhang, B. Yang, M. Liu, W. Liu, Y. Chen, Y. Wei, Polymerizable aggregation-induced emission dye-based fluorescent nanoparticles for cell imaging applications, Polym. Chem. 5 (2014) 356–360, https://doi.org/10.1039/c3py01226c.
[45] Z. Long, M. Liu, K. Wang, F. Deng, D. Xu, L. Liu, Y. Wan, X. Zhang, Y. Wei, Facile synthesis of AIE-active amphiphilic polymers: self-assembly and biological imaging applications, Mater. Sci. Eng. C Mater. Biol. Appl. 66 (2016) 215–220, https://doi.org/10.1016/j.msec.2016.04.081.
[46] R. Jiang, H. Liu, M. Liu, J. Tian, Q. Huang, H. Huang, Y. Wen, Q.Y. Cao, X. Zhang, Y. Wei, A facile one-pot Mannich reaction for the construction of fluorescent polymeric nanoparticles with aggregation-induced emission feature and their biological imaging, Mater. Sci. Eng. C Mater. Biol. Appl. 81 (2017) 416–421, https://doi.org/10.1016/j.msec.2017.08.048.
[47] R. Jiang, M. Liu, C. Li, Q. Huang, H. Huang, Q. Wan, Y. Wen, Q.Y. Cao, X. Zhang, Y. Wei, Facile fabrication of luminescent polymeric nanoparticles containing dynamic linkages via a one-pot multicomponent reaction: synthesis, aggregation-induced emission and biological imaging, Mater. Sci. Eng. C Mater. Biol. Appl. 80 (2017) 708–714, https://doi.org/10.1016/j.msec.2017.07.008.
[48] J. Chen, M. Liu, Q. Huang, L. Huang, H. Huang, F. Deng, Y. Wen, J. Tian, X. Zhang, Y. Wei, Facile preparation of fluorescent nanodiamond-based polymer composites through a metal-free photo-initiated RAFT process and their cellular imaging, Chem. Eng. J. 337 (2018) 82–90, https://doi.org/10.1016/j.cej.2017.12.085.